`

Supplementary Materials

Biomimetic Oxidation of Benzofurans with Hydrogen Peroxide catalysed by Mn(III) Porphyrins

Susana L. H. Rebelo [1,*], Sónia M. G. Pires [2], Mário M. Q. Simões [2], Baltazar de Castro [1], M. Graça P. M. S. Neves [2,*] and Craig J. Medforth [3,*]

[1] LAQV-REQUIMTE, Department of Chemistry and Biochemistry, Faculty of Sciences, University of Porto, Rua do Campo Alegre, 4169-007 Porto. E-mail: craig.medforth@fc.up.pt; susana.rebelo@fc.up.pt;

[2] QOPNA & LAQV-REQUIMTE and Department of Chemistry, University of Aveiro, 3810-193 Aveiro, Portugal; e-mail: gneves@ua.pt

[3] Department of Chemistry, University of California, One Shields Avenue, Davis, California 95616, USA; e-mail: cjmedforth@ucdavis.edu

Section 1. Comparison of catalytic activity of Mn(III) porphyrins in the oxidation of benzofurans at 0.7% loading

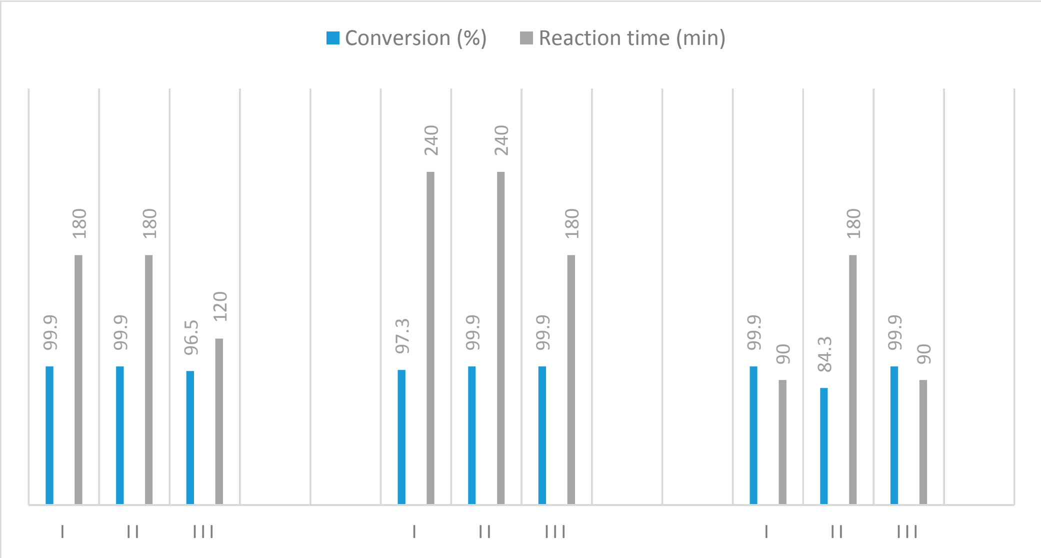

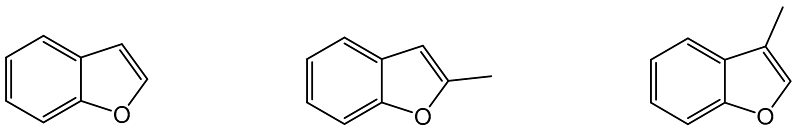

BF 2MBF 3MBF

Figure S1. Comparison of substrate conversion (%) and reaction time (min) observed during catalytic oxidation of BF, 2MBF and 3MBF in the presence of the different metalloporphyrins at a ratio S/C 150 (0.7% catalyst loading).

*Section 2. Mass spectrometry studies of **BF** and **2MBF** oxidation reactions in the presence of CAT **I***

The products formed during BF and 2MBF oxidation reactions were studied by High Resolution Mass Spectrometry with Electrospray Ionization in the positive mode (HRMS-ESI^+) with tandem studies (MS^n).

2.1 BF oxidation reactions

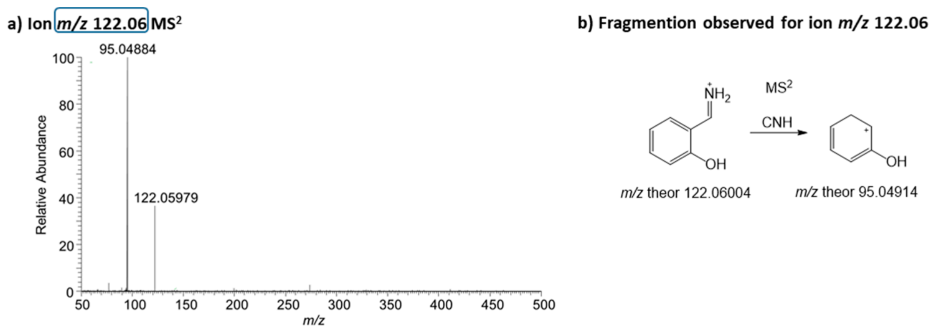

Figure S2. MS^n study of the **BF** oxidation product **1a** (ion *m/z* 122.06).

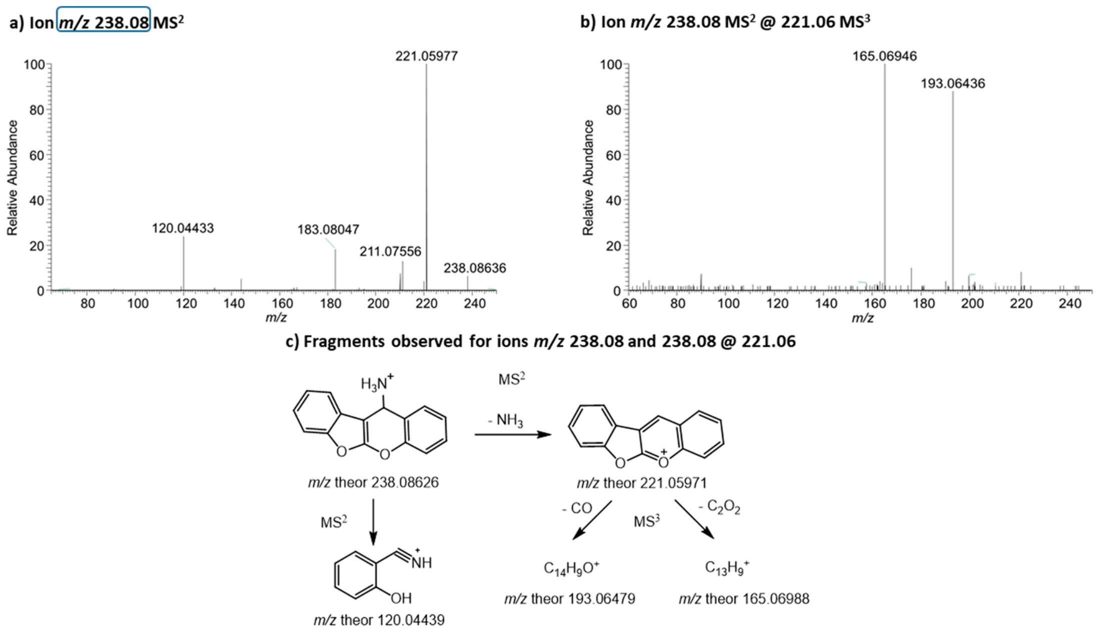

Figure S3. MS^n study of the **BF** oxidation product **2** (ion *m/z* 238.08).

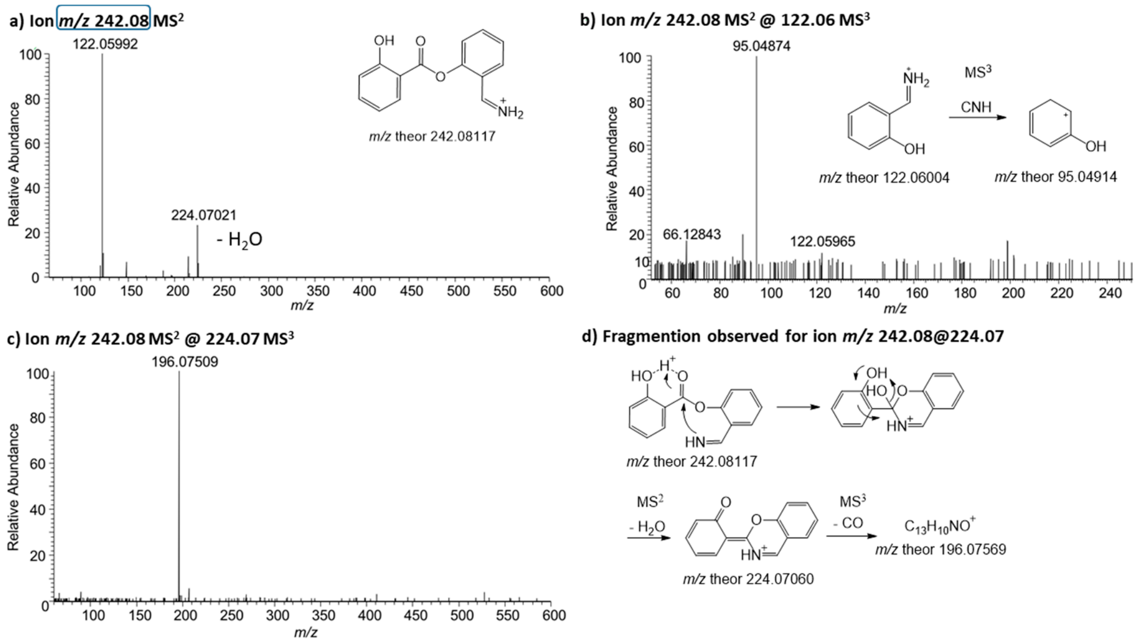

Figure S4. MS^n study of the **BF** oxidation product **3** (ion *m/z* 242.08).

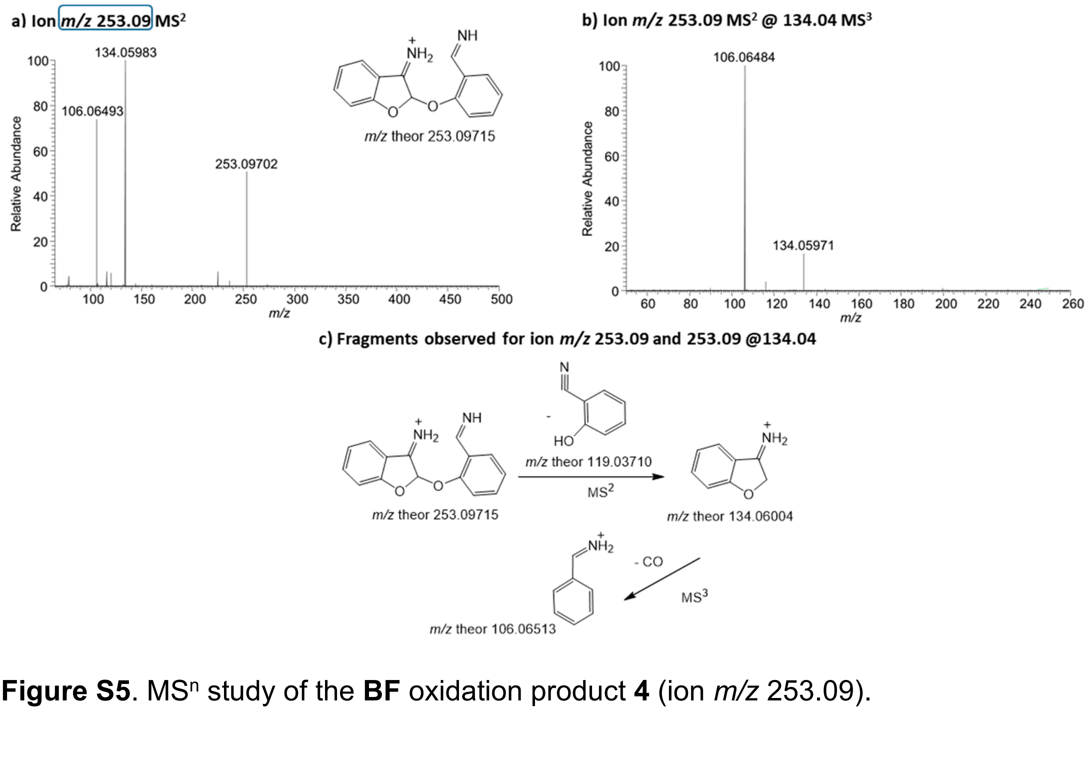

Figure S5. MS^n study of the **BF** oxidation product **4** (ion *m/z* 253.09).

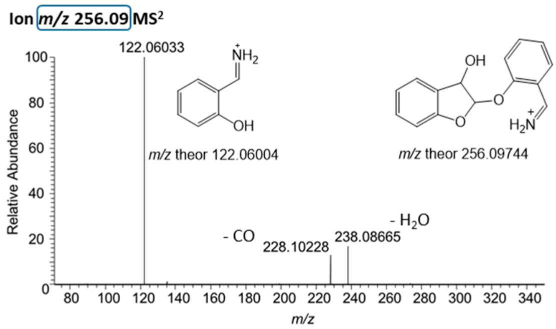

Figure S6. MS^n study of the **BF** oxidation product **5a** (ion *m/z* 256.09).

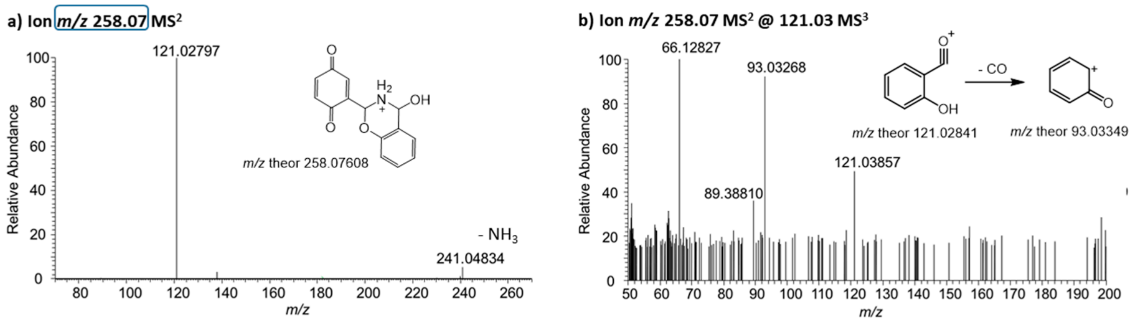

Figure S7. MS^n spectra of **BF** product **6** (ion *m/z* 258.07).

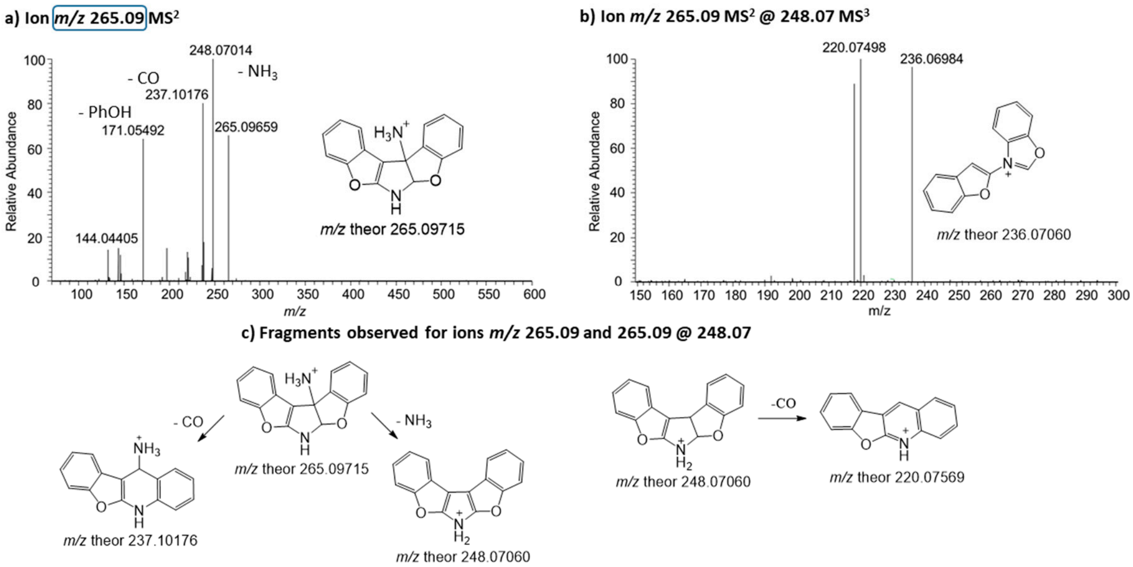

Figure S8. MS^n study of the **BF** oxidation product **7** (ion *m/z* 265.09).

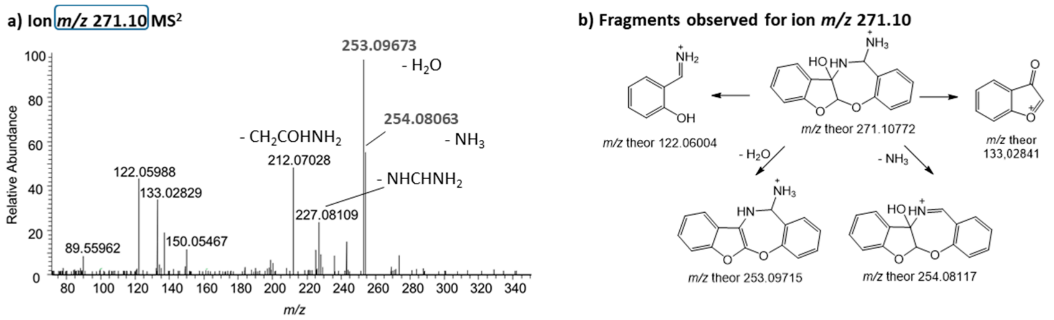

Figure S9. MS^n study of the **BF** oxidation product **8** (ion *m/z* 271.10).

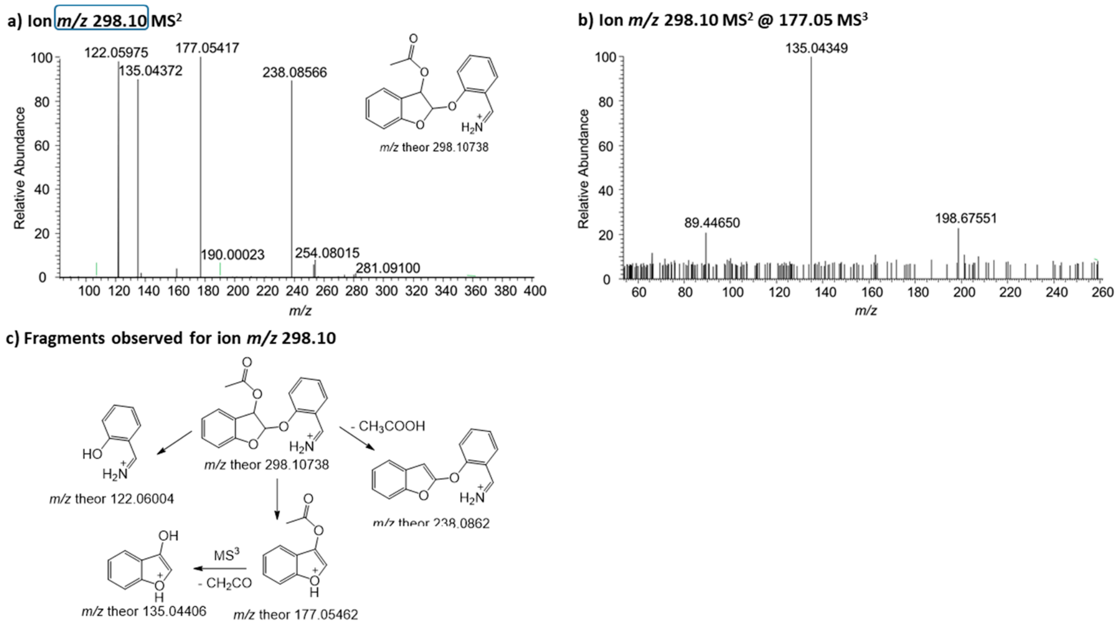

Figure S10. MS^n study of the **BF** oxidation product **9** (ion *m/z* 298.10).

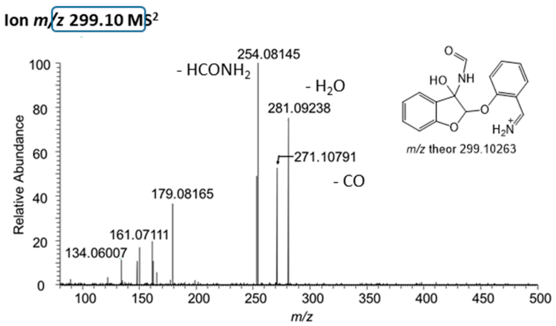

Figure S11. MS^n study of the **BF** oxidation product **10** (ion *m/z* 299.10).

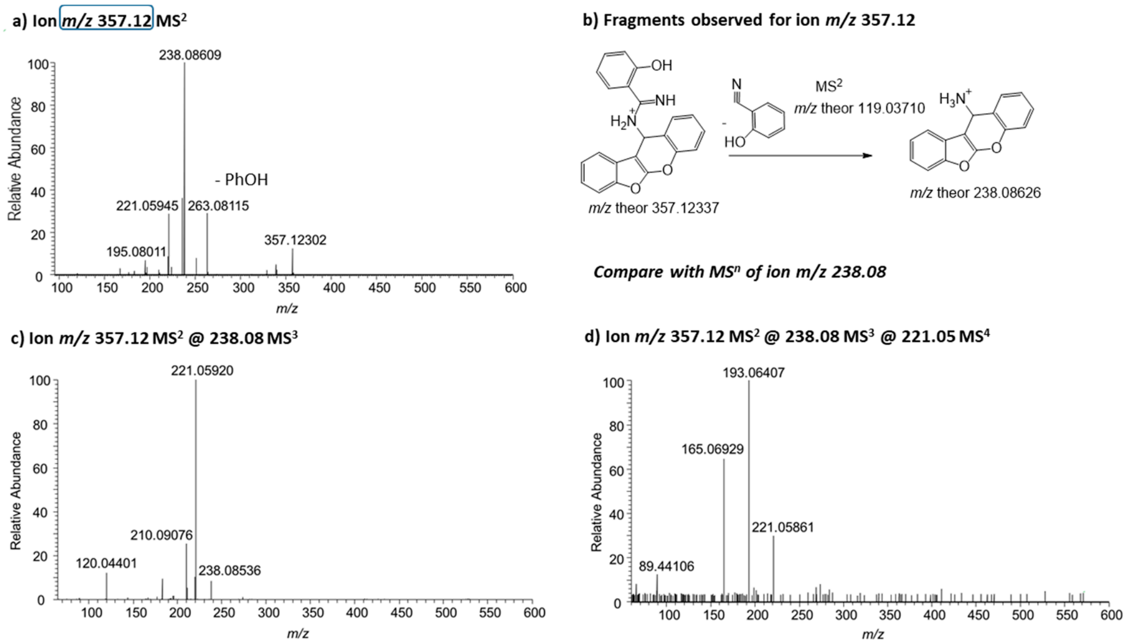

Figure S12. MS^n study of the **BF** oxidation product **11** (ion *m/z* 357.12).

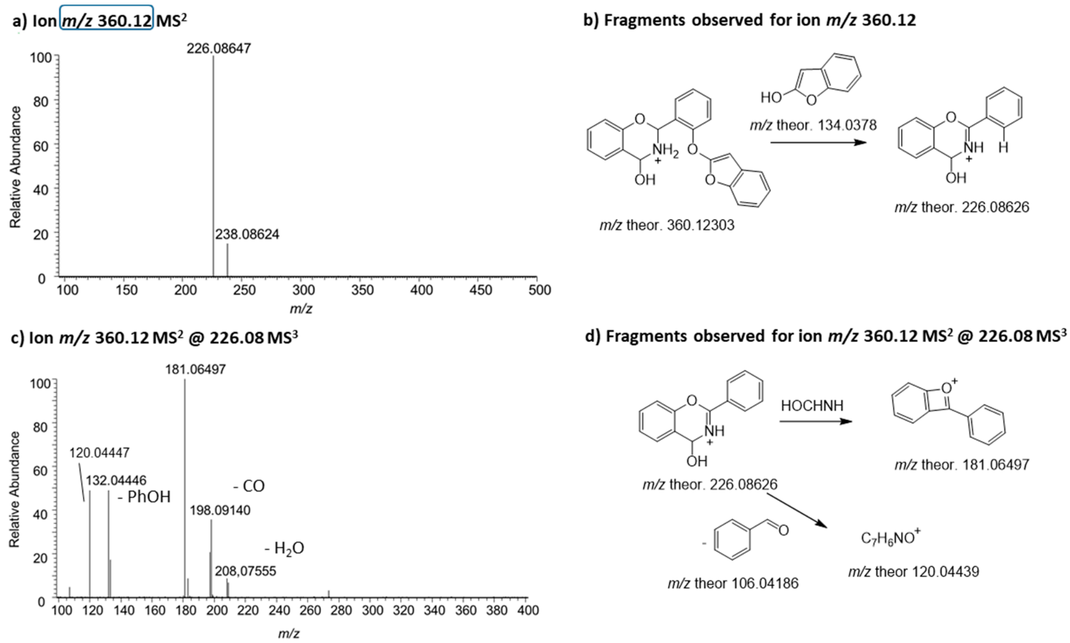

Figure S13. MS^n study of the **BF** oxidation product **12** (ion *m/z* 360.12).

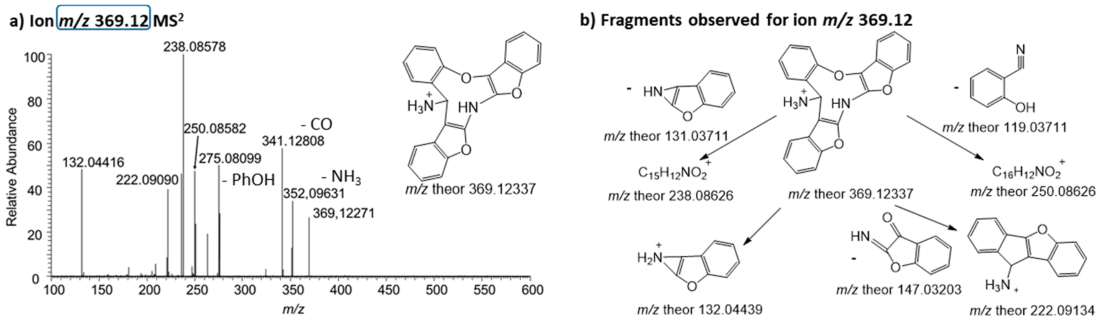

Figure S14. MS^n study of the **BF** oxidation product **13** (ion *m/z* 369.12).

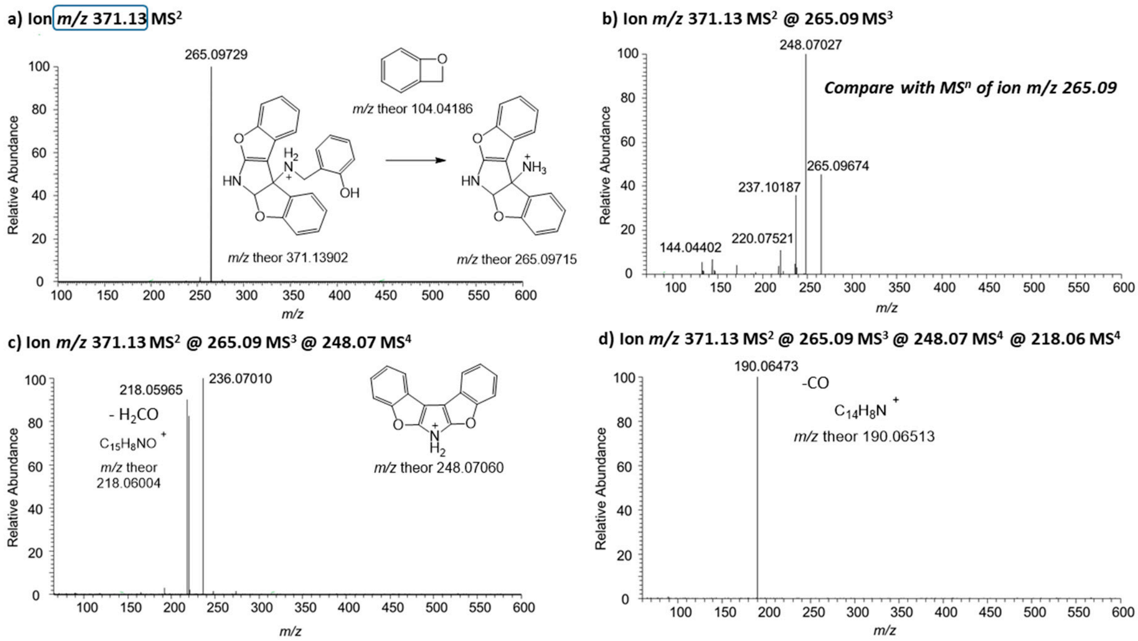

Figure S15. MS^n study of the **BF** oxidation product **14** (ion *m/z* 371.13).

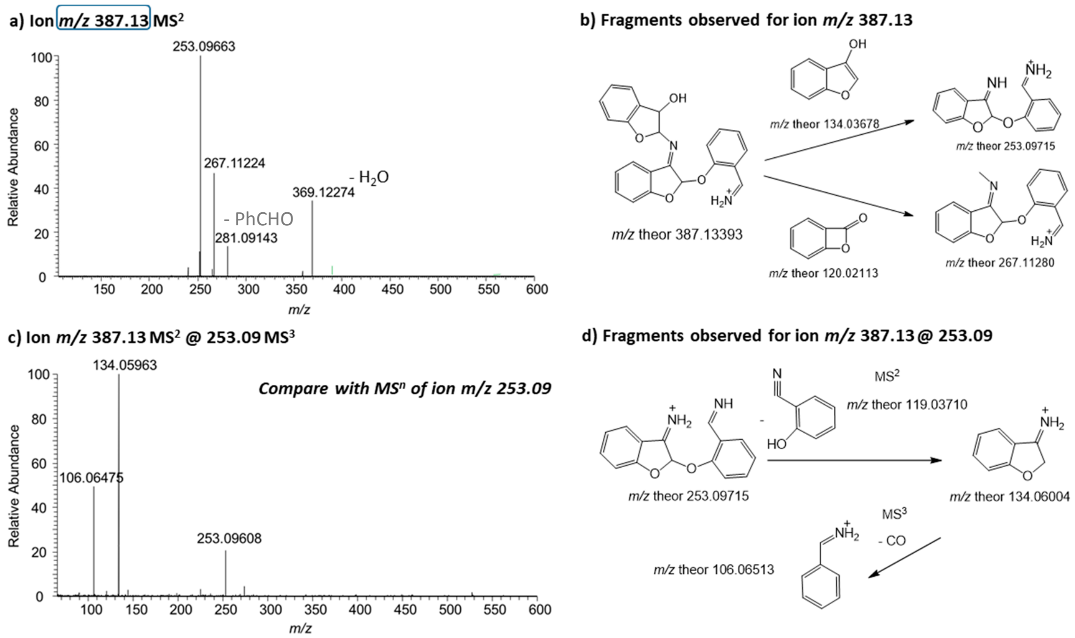

Figure S16. MS^n study of the **BF** oxidation product **15** (ion *m/z* 387.13).

2.2 2MBF oxidation reactions

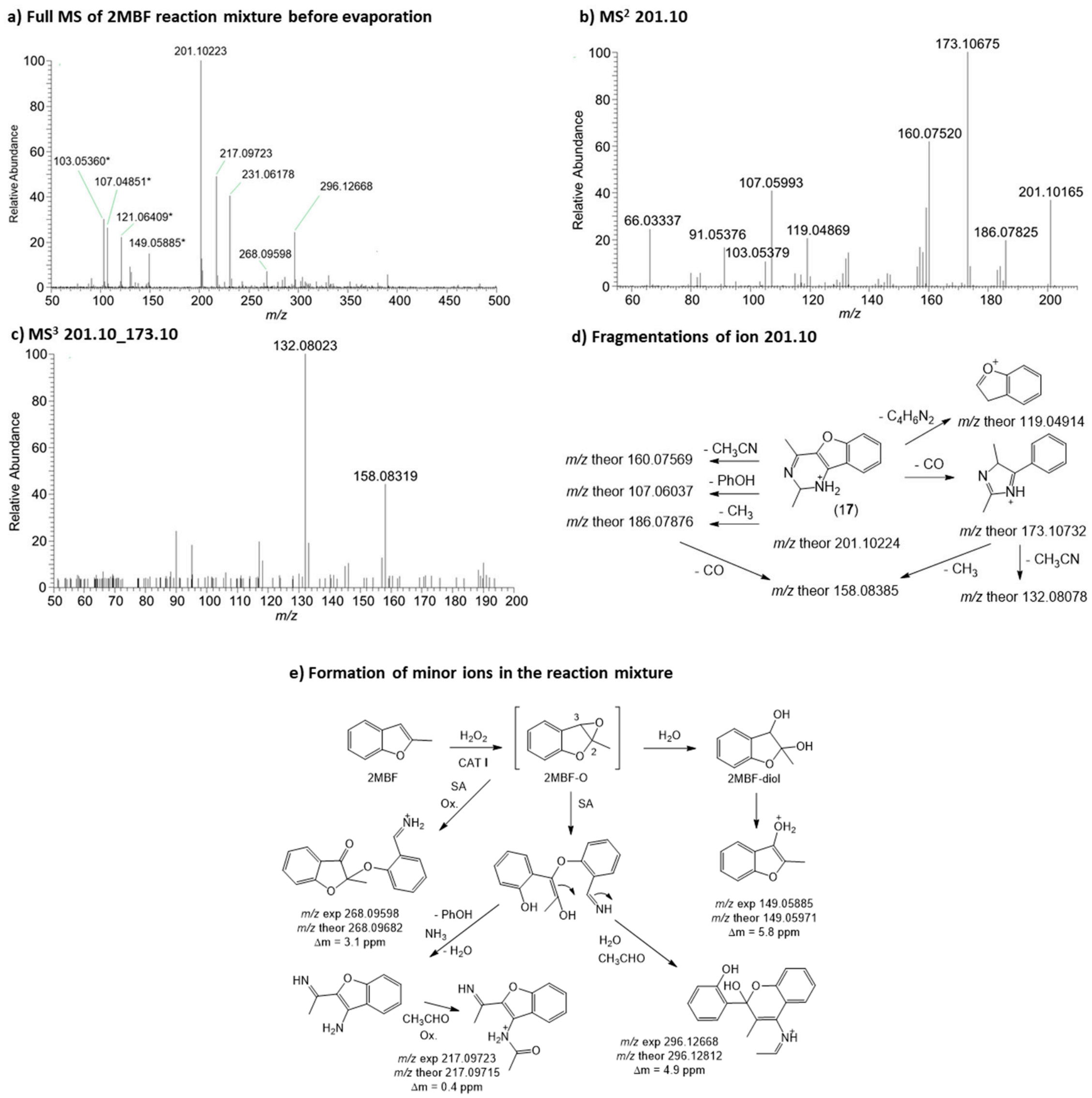

Figure S17. a) Mass spectra of 2MBF oxidation reaction using CAT **I**, Ox/S of 4 and performing solvent evaporation at 20ºC; b) – d) MS^n studies of ion *m/z* 201.10 (**17**); e) proposed mechanisms for the formation of minor ions in the **2MBF** oxidation reaction (a).

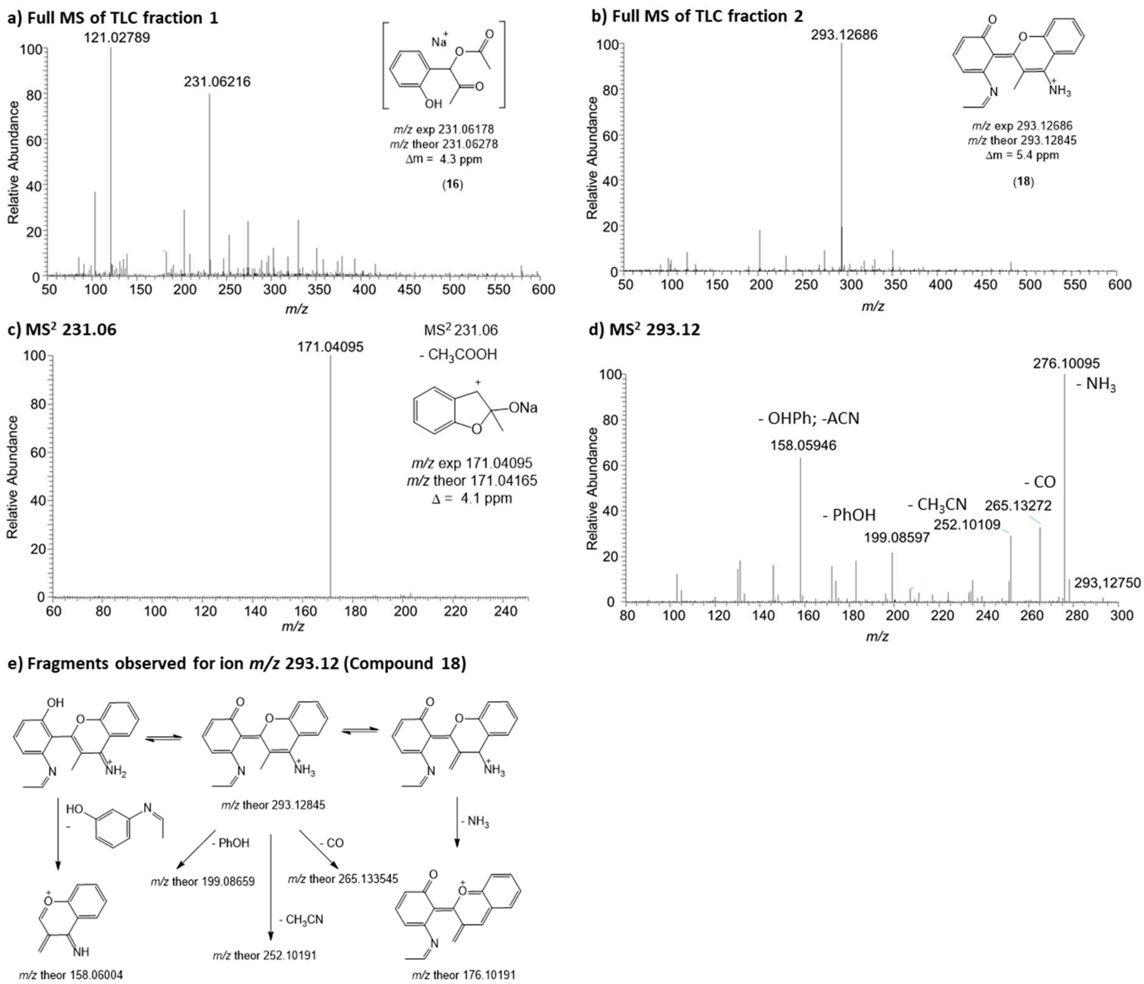

Figure S18. a) and b) MS full spectra of fractions isolated by TLC; c) – e) MS^2 studies of ions in the TLC fractions.

Section 3. NMR spectra of products and reactions mixtures

a)

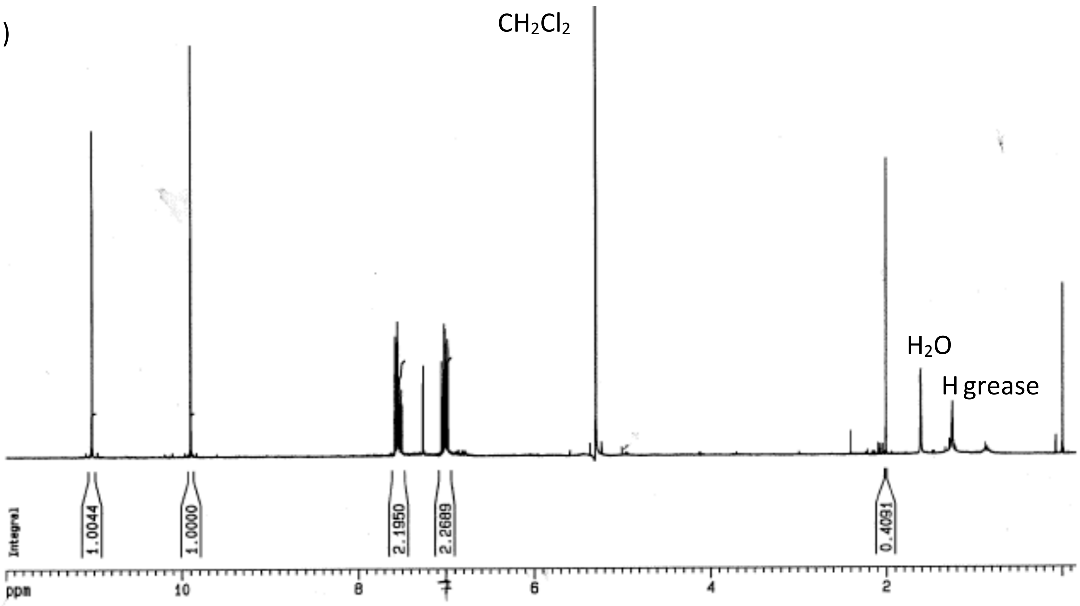

b)

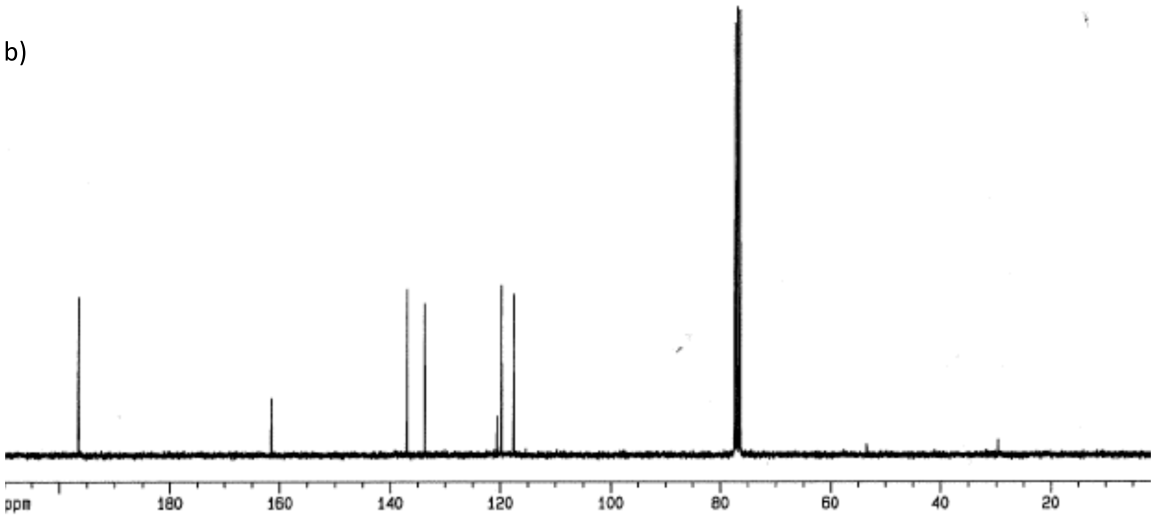

Figure S19. NMR spectra of compound **1** in $CDCl_3$: a) ^{1}H NMR; b) ^{13}C NMR .

a)

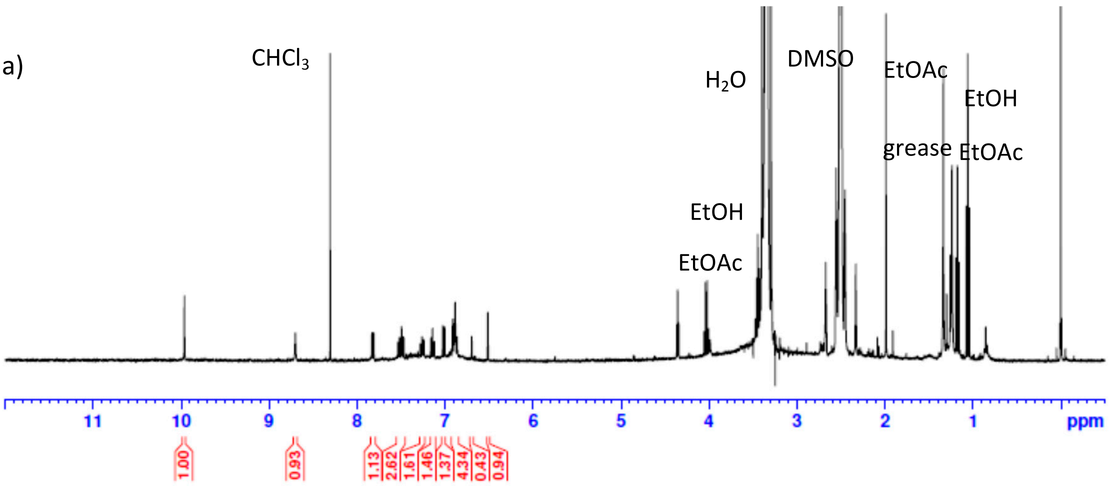

b)

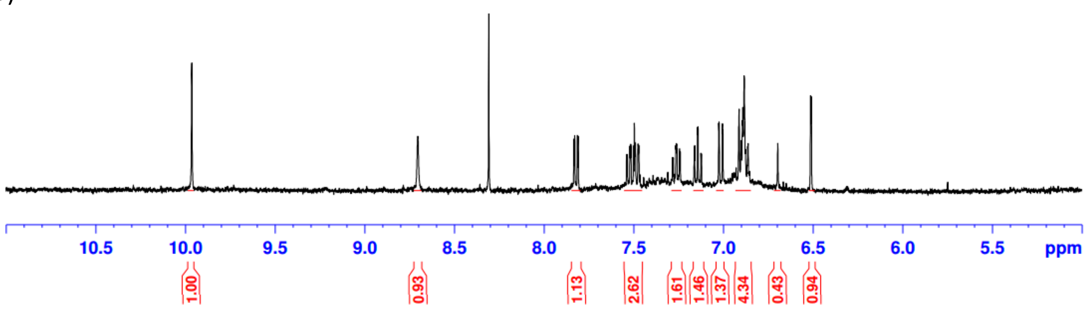

Figure S20. a) ^{1}H NMR spectrum of compound **5** in DMSO-*d*6; b) expansion in the region of 4-11 ppm.

a)

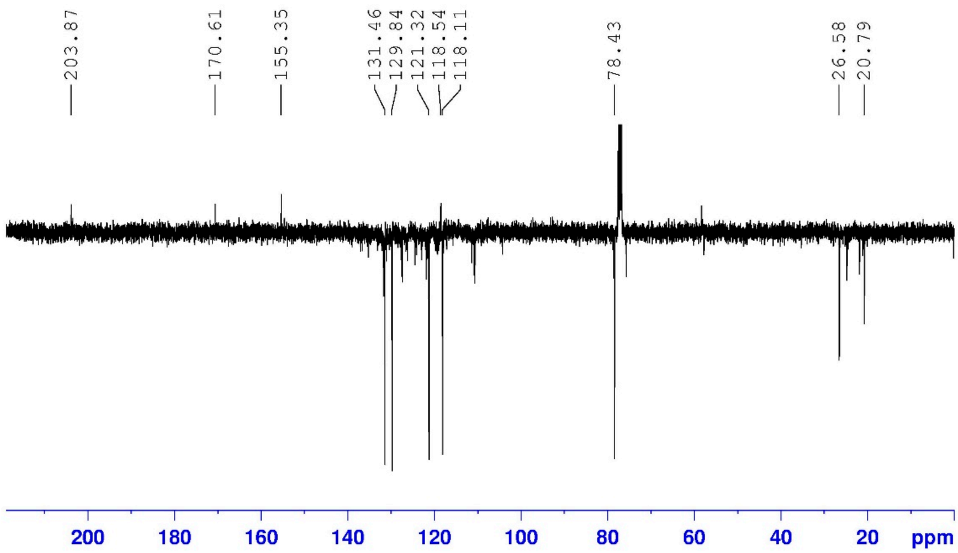

b)

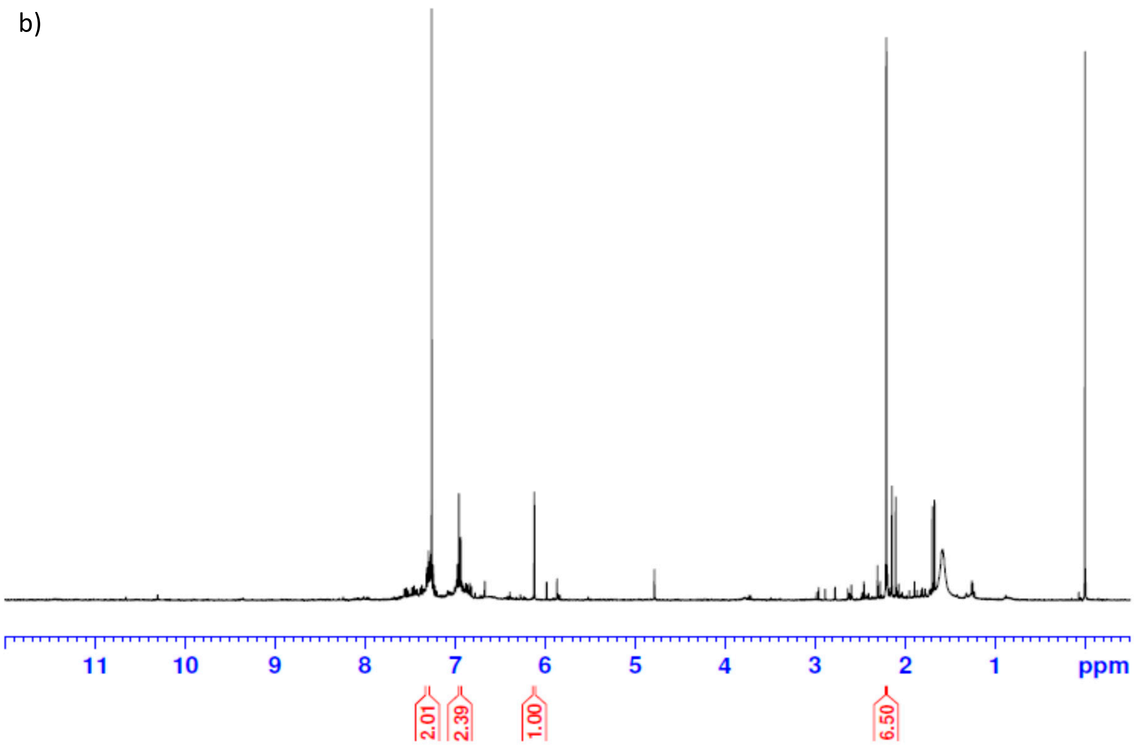

Figure S21. NMR spectra of compound **16** in $CDCl_3$: a) APT experiment (CH_2 groups and quaternary carbons are shown positive, CH_3 and CH groups are shown negative); b) ^1H NMR.

*^{1}H NMR of total reaction mixture of **3MBF** oxidation*

Figure S22 shows the ^{1}H NMR spectrum of the total reaction mixture of **3MBF** oxidation in the presence of CAT **I** and confirms the presence of two products. Two intense peaks in the aliphatic region are assigned to the methyl groups of lactone **19** (δ 1.57 ppm as a doublet) and 2'-hydroxyacetophenone **20** (δ 2.64 ppm as a singlet). The singlet at 12.3 ppm is assigned to the resonance of the hydroxyl proton of **20**.

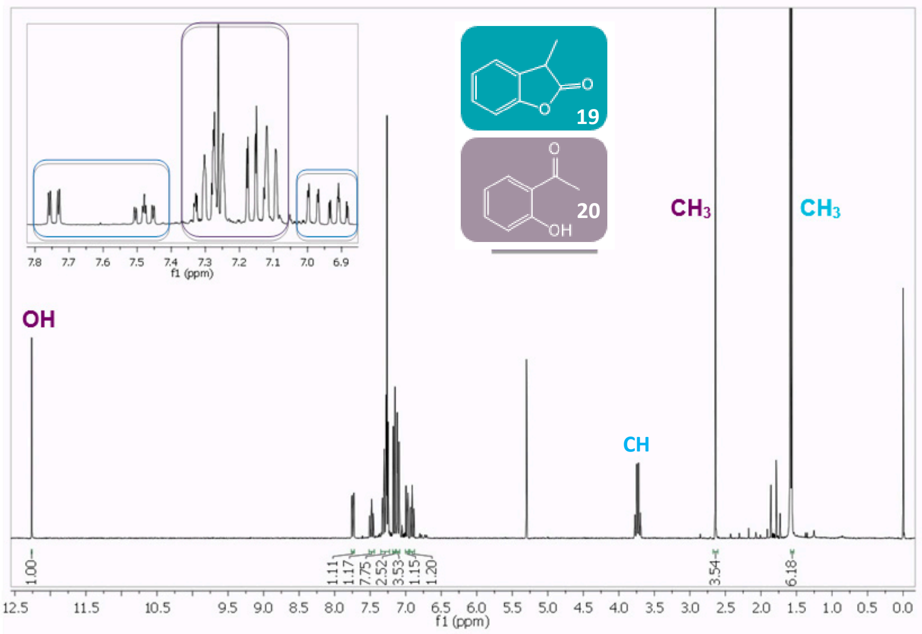

Figure S22. ^{1}H NMR spectrum in $CDCl_3$ of the total reaction mixture of **3MBF** oxidation using catalyst CAT **I** after passing through a small plug of alumina and evaporation at room temperature. The signals of compound **19** are marked in blue and the signals of compound **20** are marked in purple. Compound **20** (2´-hydroxyacetophenone) is observed in higher ratio towards the lactone **19** relatively to GC results in Table 1. This can be explained by higher volatility of the latter leading to it being partially removed during the drying process.

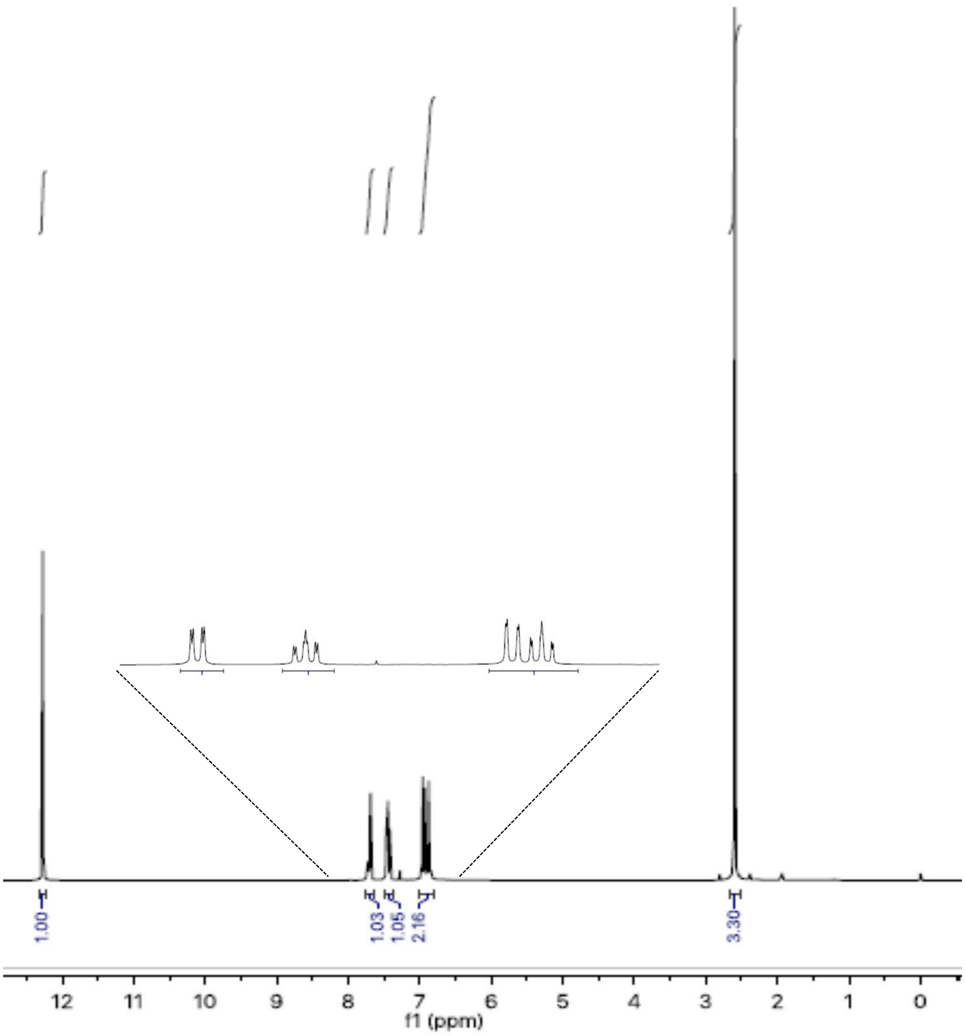

Figure S23. ^{1}H NMR spectrum of compound **20** in $CDCl_3$.

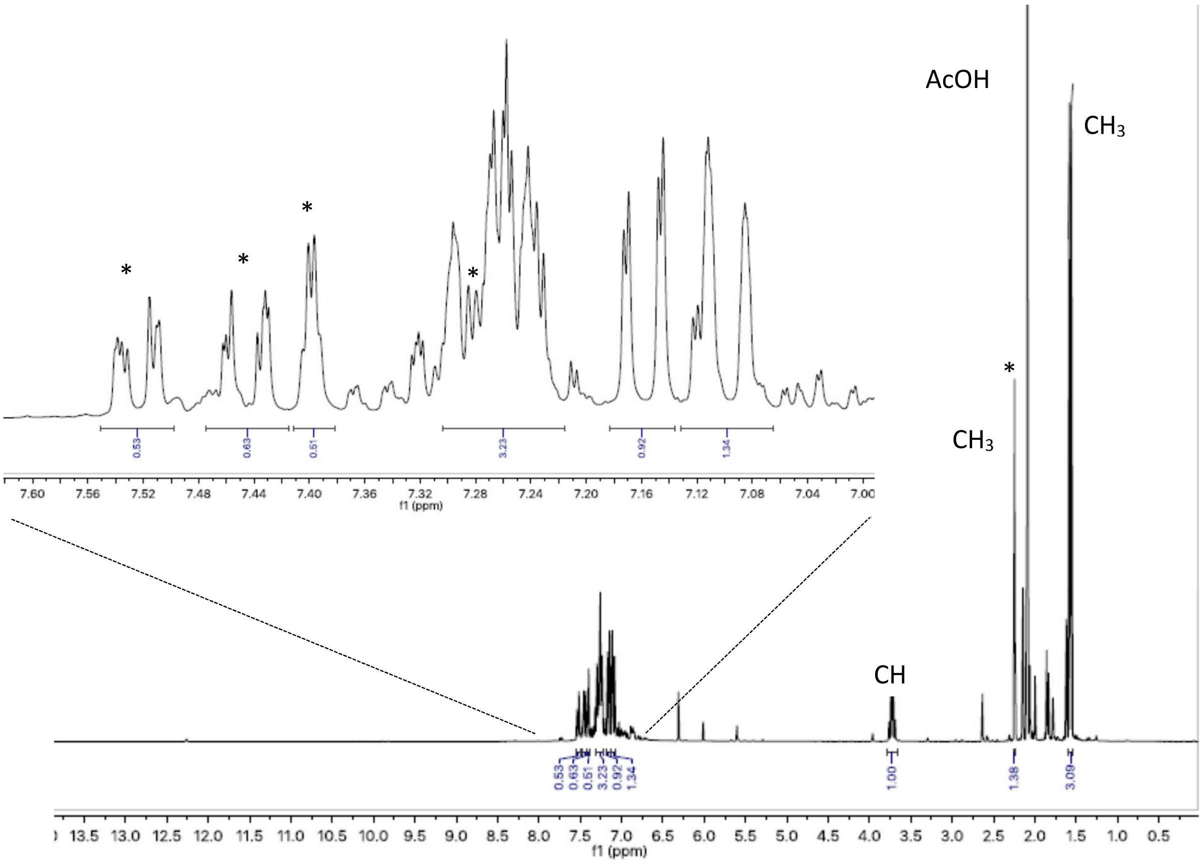

Figure S24. ^{1}H NMR spectrum in $CDCl_3$ of the total reaction mixture of **3MBF** oxidation using catalyst CAT **III** after passing through a small plug of alumina and evaporation at room temperature. In this condition, the compound **20** (2'-hydroxyacetophenone) is only detected in trace amounts but the lactone **19** is present in equilibrium with its enol form whose signals are marked with an asterisk.

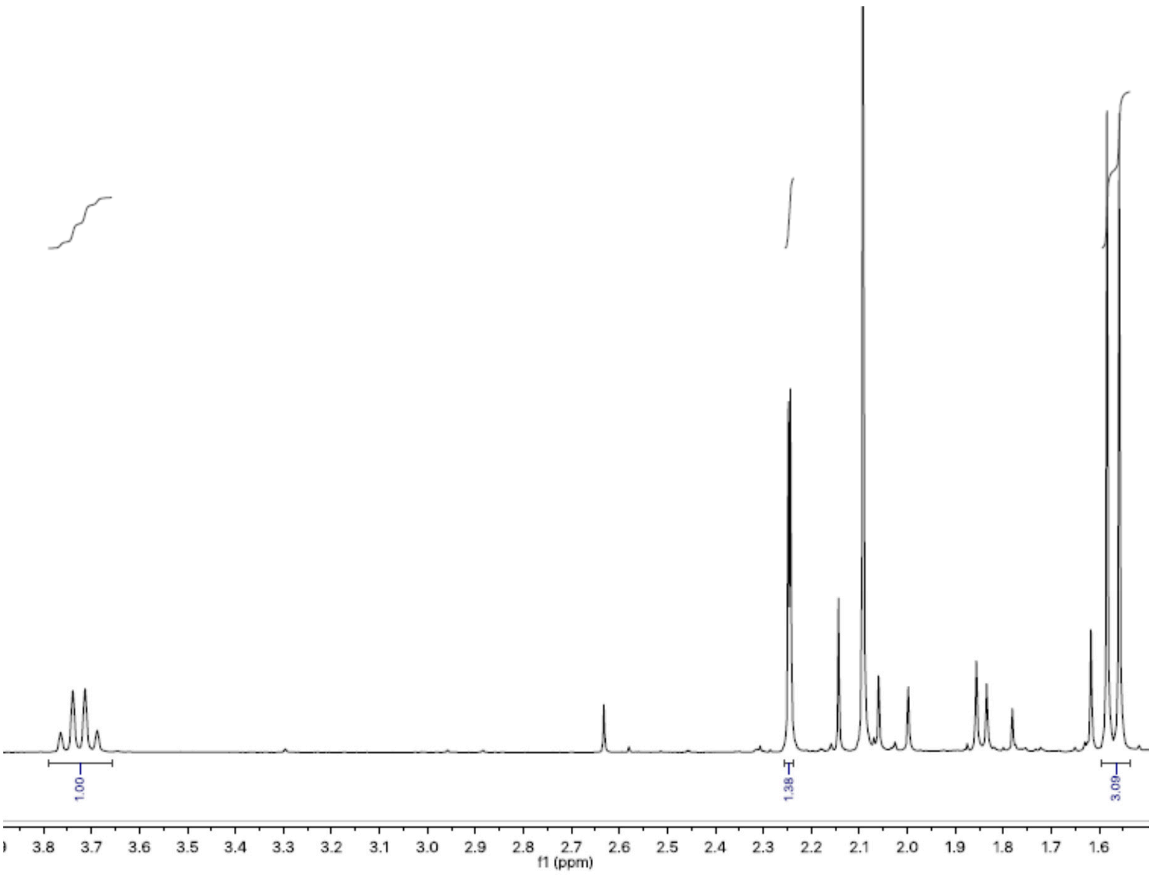

Figure S25. Expansion of [1]H NMR spectrum (1.5 – 4 ppm) of the total reaction mixture of **3MBF** oxidation using catalyst CAT **III** (in previous Figure).